



# Thermodynamics analysis of a combined cooling, heating and power system integrating compressed air energy storage and gas-steam combined cycle



Xin He, ChengChen Li, Huanran Wang <sup>\*</sup>

School of Energy and Power Engineering, Xi'an Jiaotong University, Xi'an, Shaanxi, 710049, China

## ARTICLE INFO

### Keywords:

Compressed air energy storage (CAES)  
Gas-steam combined cycle (GTCC)  
Cracking reaction of methanol  
Large-scale peak shaving capability  
Combined cooling  
Heating and power (CCHP)

## ABSTRACT

The electrical energy storage (EES) with large-scale peak shaving capability is one of the current research hot-spots. A novel combined cooling, heating and power (CCHP) system with large-scale peak shaving capability, the compressed air energy storage integrated with gas-steam combined cycle (CAES-GTCC), is proposed in this paper. In the presented system, the methanol absorbs the compression heat through the cracking reaction avoiding the application of a thermal energy storage system in compressed air energy storage (CAES) system, and the generated cracked gas is burned to drive the gas-steam combined cycle (GTCC) for generating electricity. During discharging, part of the gas diverted from the GTCC heats the air that is about to enter the air turbine in CAES to increase the total output power of the system. Moreover, the coupled system could output heating energy and cooling energy at the same time as electricity to realize the energy cascade utilization. By building the thermodynamic model of the system, the thermodynamic performance of the system and the influence of various important parameters on the performance of the system are analyzed. The results show that the output power of the CAES-GTCC during discharging accounted for 157.09% of the total output power during the general period. Furthermore, the energy efficiency of CAES-GTCC can reach 90.81% when the electrical efficiency of the CAES and equivalent electric efficiency of the CAES-GTCC are 48.07% and 74.51%, respectively. Based on the second law of thermodynamics, the exergy efficiency of the CAES-GTCC is expected to be 52.89%.

## 1. Introduction

Electrical energy storage (EES) technologies are generally regarded as an important technology for solving renewable energy grid connections and grid peak regulation at home and abroad [1]. In recent years, EES technologies have become increasingly indispensable with the rapid expansion of the scale of new energy utilization [2].

Among the existing EES technologies, compressed air energy storage (CAES) and pumped hydro energy storage (PHES) have attracted much attention due to their large energy storage capacity [3,4]. These two physical energy storage technologies have their own advantages and disadvantages. PHES is one of the most mature physical energy storage technologies with high efficiency [5–7]. However, PHES takes a long time to build. During construction, damage to the environment and ecology is inevitable [8]. Therefore, a large number of researchers are optimistic about the development of CAES. The air is stored in salt wells or caves rather than destroying the ecological environment [9]. During

charging, the air is stored in the cave by using surplus electricity or the electricity generated by renewable energy. The stored high-pressure air expands in the turbine to generate electricity during discharging [10]. After a long period of research, various types of CAES systems have been formed, including diabatic compressed air energy storage (D-CAES), adiabatic compressed air energy storage (A-CAES), isothermal compressed air energy storage (I-CAES), and liquid air energy storage (LAES), etc [11–15]. There are already two built and commercialized CAES power plants in the world, the Huntorf plant, which was built in Germany, and the McIntosh plant, which was built in America [16].

The A-CAES has received extensive attention from researchers because of its benefits of higher efficiency and simple system structure among these mentioned systems. The compression heat generated during charging is stored in the thermal energy storage system in A-CAES. The compression heat is used to heat the air entering the turbine during discharging [17]. Compared with the D-CAES, the energy efficiency of the A-CAES is significantly improved, but the application of the thermal

\* Corresponding author.

E-mail address: [huanran@xjtu.edu.cn](mailto:huanran@xjtu.edu.cn) (H. Wang).

energy storage system increases the investment. This is one of the reasons why A-CAES is not widely commercialized. As reported in the literature, the energy efficiency of A-CAES can reach 50–75% according to theoretical analysis [18–21]. In application, the CAES with thermal energy storage in Wuhu achieved an efficiency of 22.6% [22].

To improve the performance of A-CAES, the combination of A-CAES with other systems has become one of the research hotspots. Yao et al. proposed a combined cooling, heating and power (CCHP) system combining CAES with the gas engine and carried out a thermo-economic analysis of the system. It was found that the exergy efficiency of the system was 51% [23]. Chen et al. proposed a novel system combining CAES and PHES and found that the energy efficiency could reach 63% when the efficiency of hydro turbine generator units was 90% [24]. Li et al. studied a system that couples A-CAES with the Kalina Cycle. The exergy efficiency of the system could reach 47.17% after comprehensively considering the thermodynamics and economic indicators of the system [25]. Zhong et al. analyzed a novel system integrating CAES and thermochemical energy storage with oxide fuel cell-gas turbine. The proposed system could both output electricity and heating energy, and the total energy efficiency of the system could reach 89.76% [26]. DinAli et al. proposed a CCHP system that couples CAES and a single effect absorption cooling system. The study results showed that the overall energy efficiency for the multigenerational system could reach 53% whereas the overall exergy efficiency for the system remains at 41.7% [27]. Jannelli et al. conducted a thermodynamic performance evaluation of the system coupling CAES with the photovoltaic power plant, and the equivalent efficiency of the system could reach 57% [28]. Mohammadi et al. proposed a system that couples CAES and solar dish collector system, which could achieve the exergy efficiency of 53.36% [29]. Wang et al. combined CAES with the Organic Rankine Cycle. The results showed that the energy efficiency and exergy efficiency of the proposed system could reach 98.30% and 68.94% respectively, in a whole round trip cycle [30]. Most of the above-mentioned coupled systems have a large number of devices and are more expensive to manufacture.

The gas-steam combined cycle (GTCC) is a mature power generation technology that has been widely used in power plants and industrial processes [31]. GTCC has ideal efficiency, especially the efficiency of double-pressure or triple-pressure GTCC system can reach 70% [32]. Therefore, coupling CAES with GTCC is a new research route. For example, the system proposed in the literature [33] was based on the built GTCC coupled thermal energy storage to achieve the purpose of reducing the overall investment cost of the system. Salvini studied a system that couples CAES with GTCC, which could achieve efficiency values ranging from 58% to 65%. The exhaust gas of the gas turbine was diverted to an air heater to heat the compressed air before it expanded in the air turbine [34]. Kim et al. proposed a power system that couples CAES with a gas turbine. The compressed air produced from the CAES could be used by injecting it after the compression process of the gas turbine in the proposed system. The compressed air injection induced a larger increase in the output power of a turbine compared to an increase in the compressor power consumption [35]. Wojcik et al. combined GTCC with the A-CAES. During charging, the compressor in the gas cycle (GC) was acting as the first stage of the A-CAES compressor train. The remaining compressors were driven by the gas turbine shaft. This new hybrid power plant would avoid the GTCC plant gas turbine operating under the low load level [36]. The exhaust air from the CAES outlet was supplied to the bottoming steam cycle (SC) of the GTCC. Some air from the CAES high-pressure expander outlet was injected into the gas turbine combustor of the GTCC in the system proposed by Jeong et al. At the same time, the gas from the gas turbine outlet was used to heat the air entering the air turbine [37]. Yang et al. examined the system combining GTCC with CAES. The off-design models of the system were built and energy efficiency increment gained 1.015% in comparison with a corresponding optimized system without CAES [38].

In the CAES and GTCC coupled system described above, only heating

the air in the CAES with the heat in the GTCC was considered. Additionally, stored air of the CAES was supplied directly to the combustion chamber in a portion of the system to increase the net output work of the system. However, the recovery and utilization of compression heat were not complementary to GTCC.

A novel CCHP system, i.e., coupling CAES with GTCC (CAES-GTCC), may have impressive effects. To fully utilize the compression heat in CAES while avoiding the application of the thermal energy storage system, the compression heat can be absorbed by the cracking reaction of the methanol, and the cracked gas is supplied to the GTCC. On the one hand, the coupled system reduces the investment in the thermal energy storage system compared to the conventional CAES; on the other hand, the immediate use of compression heat avoids the loss of heat during storage and multiple heat exchange processes. During discharging, part of the gas diverted from the GTCC heats the air that is about to enter the air turbine in CAES to increase the total output power of the system acting as a peak regulation. In addition, the CAES-GTCC system can output various forms of energy including cooling energy, heating energy and electricity to realize the energy cascade utilization. It is worth mentioning that the CAES-GTCC can make full use of the built GTCC to reduce the total construction cost. This is expected to further improve the integration performance of the coupled system.

Regarding the feasibility of the combined system, the use of methanol for energy storage and power generation has also been a research hotspot in addition to the GTCC system that has been commercialized [39–42]. This supports the feasibility of the proposed system. This paper investigates the comprehensive performance of the proposed system based on thermodynamics, which may promote the development of EES.

The organization of this paper is as follows. Section 2 introduces the concept of the CAES integrated with GTCC in detail. Then, the thermodynamics model of related equipment is given in section 3. Section 4 conducts a sensitivity analysis to evaluate the impact of some key variables on system performance. Finally, the conclusions are drawn in Section 5.

## 2. System description

The schematic diagram of the CAES integrated with GTCC is shown in Fig. 1. CAES is mainly composed of several compressors (COM), a pump (PUM), a cavern, several turbines (TUR), several heat exchangers (HX), two cracking reactors (CR), and several throttle valves (THV). The GTCC in this paper is the conventional single-pressure no-reheat cycle.

The working process of GTCC:

GTCC is always in operation. In the GC, the air (state 18) is compressed by COM4 and then enters the combustion chamber (CC) to mix with the fuel (state 17) for combustion. The high-temperature combustion gas (state 20) expands in TUR3 to produce electricity, and the exhaust gas of TUR3 (state 21) enters the heat recovery steam generator (HRSG) to drive the SC. In the SC, the high-pressure water (state 26) pumped by PUM2 absorbs heat and evaporates in HRSG, and the superheated steam (state 27) expands in TUR4. The water-steam mixture exiting TUR4 (state 28) enters the condenser (CON) and is converted to water by releasing heat.

The working process of CAES:

During charging, the air is compressed by COM1 and COM2 in turn and stored in the cavern. The high-temperature air exhausted from COM1 and COM2 is first cooled in CR1 and CR2 respectively. In the CR1 and CR2, part of the compression heat is used to drive the cracking reaction of methanol. Then the air is cooled in HX1 and HX2 respectively. In the HX1 and HX2, the remaining compression heat is used to heat water from ambient temperature to the rated temperature for heating. Methanol is pressurized by PUM1 and then sequentially preheated by HRSG exhaust gas and exhaust mixed cracked gas of CR1 and CR2 in HX7 and HX6, respectively. The methanol is then split to CR1 and CR2 to absorb the compression heat for the cracking reaction. The cracked gas is heat exchanged with methanol in HX6 to recover the heat and then

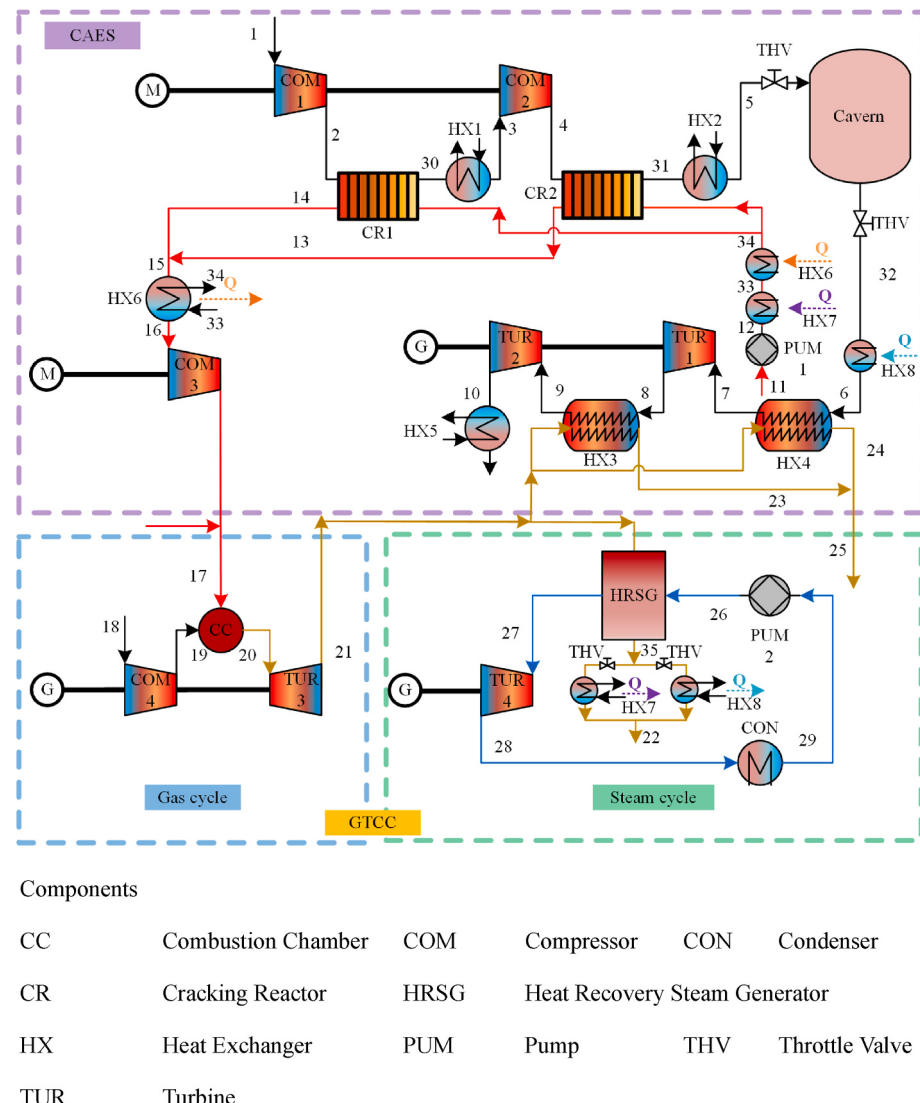


Fig. 1. Schematic of the CAES integrated with GTCC.

supplied to the CC for combustion via COM3.

During discharging, the air stored in the cavern is discharged. The air is preheated by the HRSG exhaust gas in HX8 and heated in the heat exchanger and then expands in the air turbine to produce electricity. A portion of the exhaust gas of TUR3 enters the HRSG to drive the SC, and the exhaust gas of HRSG is used to preheat the air discharged from the cavern; the other portion is introduced into HX3 and HX4 to heat the air entering TUR1 and TUR2, respectively. The exhaust air of TUR2 is used to cool water from ambient temperature to the rated temperature for cooling.

It is worth noting that the exhaust gas of HRSG exchanges heat with methanol in HX7 during the charging and the exhaust gas of HRSG exchanges heat with air in HX8 during discharging.

### 3. Model of the CAES integrated with GTCC

#### 3.1. Thermodynamic model

In this paper, the thermodynamic analysis of this system is performed by applying the steady-state analysis method. The thermodynamic model of each device in this system is described by mathematical equations. Thermodynamic parameters of all fluids in the system are obtained from REFPROP 9.1.

In order to simplify the calculations and analysis, the calculations in this paper are based on the following assumptions [33,43]:

- a. Heat losses in the combustion chamber, pipes and heat exchangers are negligible;
- b. The efficiency of all equipment in the system remains constant during operation;
- c. The temperature of the cavern is equal to the ambient temperature and remains constant;
- d. Ambient air consists of 78.12% nitrogen, 20.96% oxygen, and 0.92% argon.

#### 3.1.1. Compressor

The compression process of the compressor can be considered as an isentropic process. The pressure of the working fluid at the outlet of the compressor  $P_2$  can be expressed as:

$$P_2 = P_1 \varepsilon_{\text{COM}} \quad (1)$$

where  $\varepsilon_{\text{COM}}$  is the pressure ratio of the compressor and  $P_1$  is the pressure of the working fluid at the inlet of the compressor.

The isentropic efficiency of the compressor  $\eta_{\text{COM}}$  is defined as [44]:

$$\eta_{\text{COM}} = \frac{h_{2,s} - h_1}{h_2 - h_1} \quad (2)$$

where  $h_{2,s}$  is the specific enthalpy of the working fluid at the outlet of the compressor in the isentropic process.

The power of the compressor  $\dot{W}_{\text{COM}}$  can be written as:

$$\dot{W}_{\text{COM}} = \dot{m}_{\text{COM}}(h_2 - h_1) \quad (3)$$

where  $\dot{m}_{\text{COM}}$  is the mass flow rate of the compressor,  $h_2$  and  $h_1$  are the specific enthalpy of the working fluid at the outlet and inlet of the compressor, respectively.

### 3.1.2. Turbine

The expansion process of the turbine can be considered as an isentropic process. The pressure of the working fluid at the outlet of the turbine  $P_8$  can be calculated by:

$$P_8 = \frac{P_7}{\varepsilon_{\text{TUR}}} \quad (4)$$

where  $\varepsilon_{\text{TUR}}$  is the pressure ratio of the turbine and  $P_7$  is the pressure of the working fluid at the inlet of the turbine.

The isentropic efficiency of the turbine  $\eta_{\text{TUR}}$  is defined as [44]:

$$\eta_{\text{TUR}} = \frac{h_7 - h_8}{h_7 - h_{8,s}} \quad (5)$$

where  $h_{8,s}$  is the specific enthalpy of the working fluid at the outlet of the turbine in the isentropic process.

The power of the compressor  $\dot{W}_{\text{TUR}}$  can be obtained as:

$$\dot{W}_{\text{TUR}} = \dot{m}_{\text{TUR}}(h_7 - h_8) \quad (6)$$

where  $\dot{m}_{\text{TUR}}$  is the mass flow rate of the turbine,  $h_8$  and  $h_7$  are the specific enthalpy of the working fluid at the outlet and inlet of the turbine, respectively.

### 3.1.3. Pump

The isentropic efficiency of the pump  $\eta_{\text{PUM}}$  is written as [45]:

$$\eta_{\text{PUM}} = \frac{h_{12,s} - h_{11}}{h_{12} - h_{11}} \quad (7)$$

where  $h_{12,s}$  is the specific enthalpy of the working fluid at the outlet of the pump in the isentropic process.

The power consumed by the pump  $\dot{W}_{\text{PUM}}$  is:

$$\dot{W}_{\text{PUM}} = \dot{m}_{\text{PUM}}(h_{12} - h_{11}) \quad (8)$$

where  $\dot{m}_{\text{PUM}}$  is the mass flow rate of the pump,  $h_{12}$  and  $h_{11}$  are the specific enthalpy of the working fluid at the outlet and inlet of the pump, respectively.

### 3.1.4. Cracking reactor

The cracking reactor consists of two parts, which are the preheating section and the cracking reaction section. In the preheating section, methanol is heated to the reaction temperature. In the cracking reaction section, methanol undergoes the following cracking reactions.



In the preheating section, the thermodynamic process is the same as in the heat exchanger. In the cracking reaction section, the heat of the cracking reaction  $Q_{14}$  is calculated as follows [33,46]:

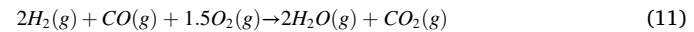
$$Q_{14} = \sum_{\text{P}} \left( \int \dot{m}_i dt \right) (\Delta H_f^0 + h_{T_p} - h_{T_0})_i - \sum_{\text{R}} \left( \int \dot{m}_j dt \right) (\Delta H_f^0 + h_{T_R} - h_{T_0})_j \quad (10)$$

where  $\Delta H_f^0$  is the standard specific enthalpy of formation,  $\dot{m}_i$  and  $\dot{m}_j$  are, respectively, the mass flow rate of product and reactant,  $h_{T_p}$  is the thermodynamic specific enthalpy of reactant,  $h_{T_p}$  is the thermodynamic specific enthalpy of product, and  $h_{T_0}$  is the specific enthalpy in reference state of thermochemical standard.

The cracking temperature is 250° Celsius in this paper and the equilibrium conversion of methanol is over 99% [47]. Therefore, it is considered that methanol can be cracked completely during the calculation.

### 3.1.5. Combustion chamber

The following combustion reactions occur in the combustion chamber and the air is heated to a high temperature.



The heat of the combustion reaction  $Q_c$  is calculated in the same way as equation (10) and is expressed as follows [46]:

$$Q_c = \sum_{\text{P}} \left( \int \dot{m}_i dt \right) (\Delta H_f^0 + h_{T_p} - h_{T_0})_i - \sum_{\text{R}} \left( \int \dot{m}_j dt \right) (\Delta H_f^0 + h_{T_R} - h_{T_0})_j \quad (12)$$

The mass flow rate of the combustion chamber  $\dot{m}_{20}$  is described as:

$$\dot{m}_{20} = \dot{m}_{20,c} + \dot{m}_{20,a} \quad (13)$$

where  $\dot{m}_{20,c}$  is the mass flow rate of exhaust gas produced by the combustion of the cracked gas and  $\dot{m}_{20,a}$  is the mass flow rate of air that did not participate in the combustion reaction.

The energy balance equation in the combustion chamber can be written as:

$$\dot{m}_{20,c}(-q_c) = \dot{m}_{20,a}(h_{20,a} - h_{19,a}) \quad (14)$$

where  $q_c$  is the heat of combustion reaction per unit mass of the reactant,  $h_{20,a}$  and  $h_{19,a}$  are the specific enthalpy of the air at the outlet and inlet of the combustion chamber, respectively.

The heat of combustion reaction per unit mass of the reactant  $q_c$  is:

$$q_c = \frac{Q_c}{\sum_{\text{R}} (\int \dot{m}_j dt)} \quad (15)$$

### 3.1.6. Heat recovery steam generator and heat exchanger

The HRSG consists of three parts: superheater, evaporator and economizer. The HRSG can be simplified to three heat exchangers under the condition that the approach temperature difference and the pinch temperature difference meet the design requirements. In the heat exchanger, the first law of thermodynamics is satisfied [48].

$$\dot{m}_{23}(h_{21} - h_{23}) = \dot{m}_8(h_9 - h_8) \quad (16)$$

where  $\dot{m}_{23}$  and  $\dot{m}_8$  are the mass flow rate of the hot fluid and cold fluid, respectively.

### 3.1.7. Condenser

The two-phase mixture of water and steam at the outlet of the steam turbine is cooled to liquid water in the condenser. The heat output per unit mass of fluid in the condenser  $q_{\text{CON}}$  is expressed as:

$$q_{\text{CON}} = h_{28} - h_{29} \quad (17)$$

where  $h_{29}$  and  $h_{28}$  are the specific enthalpy of the fluid at the outlet and inlet of the condenser, respectively.

## 3.2. System performance criteria

### 3.2.1. The electrical efficiency of the CAES

The electrical efficiency of the CAES  $\eta_{\text{CAES}}$  is defined as the ratio of

total output work to total input work of CAES, which reveals the degree of electricity conversion in the CAES during charging and discharging. The expression is as follows [24]:

$$\eta_{\text{CAES}} = \frac{W_{\text{CAES,output}}}{W_{\text{CAES,input}}} \quad (18)$$

while the total output work and total input work of CAES are calculated as follows:

$$W_{\text{CAES,output}} = W_{\text{TUR1}} + W_{\text{TUR2}} \quad (19)$$

$$W_{\text{CAES,input}} = W_{\text{COM1}} + W_{\text{COM2}} + W_{\text{COM3}} + W_{\text{PUM1}} \quad (20)$$

where  $W_{\text{TUR1}}$  and  $W_{\text{TUR2}}$  are the total output work of TUR1 and TUR2, respectively.  $W_{\text{COM1}}$ ,  $W_{\text{COM2}}$  and  $W_{\text{COM3}}$  are the total input work of COM1, COM2, and COM3 respectively.  $W_{\text{PUM1}}$  is total input work of PUM1.

### 3.2.2. The equivalent electric efficiency of the CAES integrated with GTCC

The equivalent electric efficiency of the CAES-GTCC reflects the relationship between the total output work and the input work of the whole coupled system. The equivalent electric efficiency of the CAES-GTCC  $\eta_{\text{CAES-GTCC,sys}}$  is described as [49]:

$$\eta_{\text{CAES-GTCC,sys}} = \frac{W_{\text{CAES,output}} + W_{\text{GTCC,output}}}{W_{\text{CAES,input}} + M_{\text{CH}} \bullet LHV \bullet \eta_{\text{sys}}} \quad (21)$$

where  $W_{\text{GTCC,output}}$  is the total net output work of the GTCC,  $M_{\text{CH}}$  is the total mass of methanol supplied during charging, and  $LHV$  is the low heating value of methanol.  $\eta_{\text{sys}}$  is the conversion coefficient, which implies the average conversion efficiency of converting a certain fuel to work. In the paper, the conversion coefficient is set to 0.4.

The total net output work of the GTCC  $W_{\text{GTCC,output}}$  can be calculated as follows:

$$W_{\text{GTCC,output}} = (W_{\text{TUR3}} - W_{\text{COM4}}) + (W_{\text{TUR4}} - W_{\text{PUM2}}) \quad (22)$$

where  $W_{\text{TUR3}}$  and  $W_{\text{TUR4}}$  are the total output work of TUR3 and TUR4, respectively.  $W_{\text{COM4}}$  is the total input work of COM4, and  $W_{\text{PUM2}}$  is the total input work of PUM1.

### 3.2.3. The energy efficiency of the CAES integrated with GTCC

The energy efficiency of the CAES-GTCC  $\eta_{\text{CAES-GTCC}}$  is the ratio of the whole useful energy of the proposed system (electricity, heating energy and cooling energy) and all the input energy (electricity energy and fuel) based on the first law of thermodynamics [23]:

$$\eta_{\text{CAES-GTCC}} = \frac{W_{\text{CAES,output}} + W_{\text{GTCC,output}} + Q_{\text{heating}} + Q_{\text{cooling}}}{W_{\text{CAES,input}} + M_{\text{CH}} \bullet LHV} \quad (23)$$

where  $Q_{\text{heating}}$  is the total output heating energy, and  $Q_{\text{cooling}}$  is the total output cooling energy.

### 3.2.4. The exergy efficiency of the CAES integrated with GTCC

Exergy is the maximum useful work accomplished during a process, which considers the quality of energy from the perspective of the second law of thermodynamics. The exergy analysis can provide a more comprehensive and rational assessment of the system. The exergy efficiency of the CAES-GTCC  $\eta_E$  can be calculated by Ref. [23]:

$$\eta_E = \frac{E_{\text{CAES-GTCC,output}} + E_{\text{heating}} + E_{\text{cooling}}}{E_{\text{CAES,input}} + E_{\text{CH}}} \quad (24)$$

where  $E_{\text{CAES-GTCC,output}}$  is the exergy of total output power,  $E_{\text{heating}}$  is the exergy gain during heating,  $E_{\text{cooling}}$  is the exergy gain during cooling,  $E_{\text{CAES,input}}$  is the exergy of total input power, and  $E_{\text{CH}}$  is the exergy of input fuel.

The exergy of total output power consists of two parts: the exergy of

the output power of CAES and the exergy of the output power of GTCC. It can be expressed as:

$$E_{\text{CAES-GTCC,output}} = E_{\text{CAES,output}} + E_{\text{GTCC,output}} \quad (25)$$

The exergy of input fuel  $E_{\text{CH}}$  can be written as [50,51]:

$$E_{\text{CH}} = M_{\text{CH}} \bullet LHV \bullet \varphi_{\text{CH}} \quad (26)$$

while the exergy factor of fuel  $\varphi_{\text{CH}}$  can be calculated as follows:

$$\varphi_{\text{CH}} = 1.0038 + 0.1365 \frac{\omega(\text{H})}{\omega(\text{C})} + 0.0308 \frac{\omega(\text{O})}{\omega(\text{C})} + 0.0104 \frac{\omega(\text{S})}{\omega(\text{C})} \quad (27)$$

where  $\omega(\text{H})$  is the mass fraction of hydrogen in the fuel,  $\omega(\text{C})$  is the mass fraction of carbon in the fuel,  $\omega(\text{O})$  is the mass fraction of oxygen in the fuel, and  $\omega(\text{S})$  is the mass fraction of sulfur in the fuel [50].

## 4. Results and discussion

The results of the thermodynamics and sensitivity analysis of the proposed CAES integrated with GTCC are presented. In order to verify the reliability of the calculated results, the GTCC part of this simulation program is compared with the data in the literature [33]. With the same parameter settings, the efficiency of GTCC in the literature [33] is 50.85% and the simulation result of this program is 48.09%. The calculated results are close to the comparison data with an error within 3%. This is mainly due to the fact that the pressure loss is considered in the calculation of this paper while it is not considered in the comparative literature. In general, the calculation is credible. Table 1 gives the relevant parameters of the system simulation calculation. Among them, some parameters of the gas turbine are taken from the design parameters of an actual gas turbine. Table 2 shows the state points and thermodynamic properties of the system during charging and discharging, respectively. If the thermodynamic values of the state points during charging and discharging are the same, only one value is given, and ‘-’ means that no corresponding working fluid passes through the state point in that period. The relevant equipment parameters of the CAES-GTCC are listed in Table 3. Table 4 shows the logarithmic mean temperature difference of each heat exchanger in the proposed system. The calculated results show that the efficiency of SC is 32.76%, the

**Table 1**  
Parameter specification of the CAES integrated with GTCC.

Parameters	Unit	Value
Ambient temperature	K	293.15
Ambient pressure	MPa	0.101
Pressure ratio of the gas cycle	-	15
Inlet temperature of the gas turbine	K	1430.00
Isentropic efficiency of the gas turbine	-	0.85
Isentropic efficiency of the compressor	-	0.85
Isentropic efficiency of the air turbine	-	0.85
Inlet temperature of the steam turbine	K	765.00
Inlet pressure of the steam turbine	MPa	4.000
Outlet pressure of the steam turbine	MPa	0.005
Isentropic efficiency of the steam turbine	-	0.85
Isentropic efficiency of the pump	-	0.90
Approach temperature difference	K	10.00
Pinch temperature difference	K	15.28
Pressure drop coefficient	-	0.03
Reaction temperature of the cracking reaction	K	523.15
Reaction pressure of the cracking reaction	MPa	0.300
Inlet pressure of the cavern	MPa	7.200
Outlet pressure of the cavern	MPa	4.200
Cooling water initial temperature	K	293.15
Heating water initial temperature	K	293.15
Cooling water supply temperature	K	283.15
Heating water supply temperature	K	363.15
Low heating value of methanol	J/kg	19937000
Energy store time	h	8
Energy discharge time	h	8

**Table 2**

Thermodynamic properties of the states along the system (charging\discharging).

State number	Fluid	Temperature (K)	Pressure (MPa)	Mass flow rate (kg/s)
1	Air	293.15\~	0.101\~	380.72\~
2	Air	583.22\~	0.879\~	380.72\~
3	Air	308.15\~	0.853\~	380.72\~
4	Air	613.73\~	7.423\~	380.72\~
5	Air	308.15\~	7.200\~	380.72\~
6	Air	\~371.98	\~4.200	\~380.72
7	Air	\~464.34	\~4.074	\~380.72
8	Air	\~302.89	\~0.651	\~380.72
9	Air	\~411.02	\~0.632	\~380.72
10	Air	\~268.60	\~0.101	\~380.72
11	Methanol	293.15\~	0.101\~	13.00\~
12	Methanol	293.20\~	0.309\~	13.00\~
13	Cracked gas	523.15\~	0.300\~	6.50\~
14	Cracked gas	523.15\~	0.300\~	6.50\~
15	Cracked gas	523.15\~	0.300\~	13.00\~
16	Cracked gas	378.94\~	0.300\~	13.00\~
17	Cracked gas	637.59	1.515	13.00
18	Air	293.15	0.101	335.08
19	Air	684.61	1.515	335.08
20	Gas	1430.00	1.470	348.08
21	Gas	861.39	0.104	348.08
22	Gas	371.42\~303.15	0.101	348.08\~208.85
23	Gas	\~312.89	\~0.101	\~69.62
24	Gas	\~381.98	\~0.101	\~69.62
25	Gas	\~347.51	\~0.101	\~139.23
26	Water	305.69	4.124	52.73\~31.64
27	Steam	765.00	4.000	52.73\~31.64
28	Water/	306.02	0.005	52.73\~31.64
29	Steam			
30	Water	305.48	0.005	52.73\~31.64
31	Air	532.45\~	0.853\~	380.72\~
32	Air	564.22\~	7.200\~	380.72\~
33	Air	\~293.15	\~4.200	\~380.72
34	Methanol	368.94\~	0.309\~	13.00\~
35	Methanol	501.58\~	0.309\~	13.00\~
	Gas	411.48	0.101	348.08\~208.85

**Table 3**

Relevant equipment parameters of the CAES integrated with GTCC.

Parameters	Unit	Value
Power of the TUR1	kW	61791.8
Power of the TUR2	kW	54526.4
Power of the TUR3	kW	242549.1
Power of the TUR4	kW	57025.6
Power of the PUM1	kW	3.8
Power of the PUM2	kW	242.3
Power of the COM1	kW	112824.4
Power of the COM2	kW	119905.5
Power of the COM3	kW	9267.1
Power of the COM4	kW	135394.6
Power of the HRSG	kW	173327.8
Inner diameter of the CR tube	mm	66.0
Volume of the heating water	m <sup>3</sup>	19545
Volume of the cooling water	m <sup>3</sup>	3833

**Table 4**

Logarithmic mean temperature difference of each heat exchanger.

Equipment	Unit	Value
HX1	K	63.67
HX2	K	71.69
HX3	K	115.66
HX4	K	105.13
HX5	K	12.13
HX6	K	15.05
HX7	K	58.58
HX8	K	21.47

efficiency of GC is 31.43%, and the efficiency of GTCC is 48.09%.

#### 4.1. Output power, heating energy and cooling energy of the CAES-GTCC

The total output power of the CAES-GTCC at different time periods is given in Fig. 2. It should be noted that the CAES operation periods are divided into three time periods, which are the charging period, the resting period and the discharging period. The ‘General period’ in the figure refers to the time periods other than the discharging period, including the charging period and the resting period of CAES. The percentage of the output power, heating energy and cooling energy of the coupled system is shown in Fig. 3. During charging, a part of the compressed heat of COM1 and COM2 is used for output heating energy. During discharging, the temperature of the air at the outlet of TUR2 is lower than the ambient temperature and the coupled system output cooling energy. The GTCC is always in operation so that the total output power of the CAES-GTCC is the sum of the net output power of the GC and the net output power of the SC while the CAES does not output power during the general period. During discharging, the total output power of the CAES-GTCC is the sum of the net output power of the GTCC and the output power of the CAES. The output power of the CAES consists of two parts: the output power of the TUR1 and the output power of the TUR2. It is worth noting that the exhaust gas of TUR3 is partially diverted for heating the air entering TUR1 and TUR2 during the discharging period. The net output power of the SC is reduced, but the total output power of CAES-GTCC accounted for 157.09% of the total output power during the general period. More specifically, the minimum steady power capacity and the maximum capacity of the CAES-GTCC are 163.94 MW and 257.54 MW, respectively.

#### 4.2. Flow rate ratio of exhaust gas diverted from the HRSG

The flow rate ratio of exhaust gas diverted from the HRSG is the proportion of the mass of exhaust gas used to heat the air in the CAES to the total mass of exhaust gas exiting from TUR3. It can be expressed as:  $X = \frac{m_{25}}{m_{21}}$ . The effect of the flow rate ratio of exhaust gas diverted from the HRSG on the system performance is illustrated in Fig. 4. When the X is increasing, the electrical efficiency of the CAES increases; the equivalent electric efficiency of the CAES-GTCC, the energy efficiency of the CAES-GTCC and the exergy efficiency of the CAES-GTCC decrease at first and then go up. As the X increases, the mass flow rate of exhaust gas used to drive the SC decreases, and the total output work of TUR4 decreases.

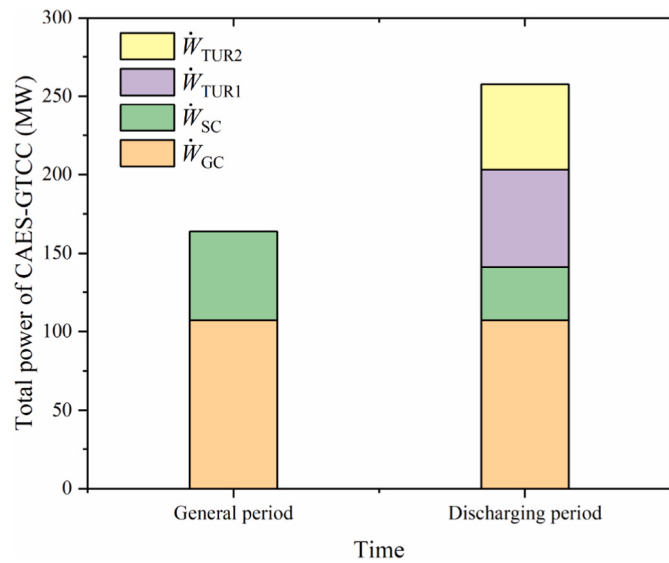
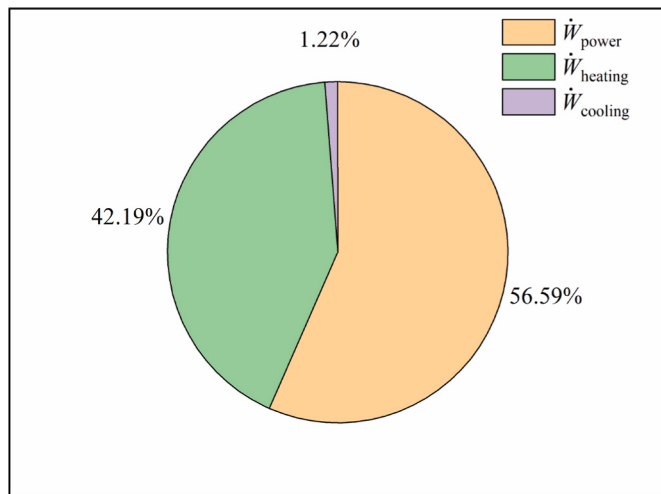


Fig. 2. Total output power of CAES-GTCC at different time periods.



**Fig. 3.** Percentage of the output power, heating energy and cooling energy of the CAES-GTCC.

Instead, the total output work of TUR1 and TUR2 increases. Therefore, the electrical efficiency of the CAES increases. Since the total output work of the CAES-GTCC decreases at first but it increases when the X reaches 0.4, the equivalent electric efficiency of the CAES-GTCC decreases at first and then goes up. The increase of the X does not affect the output heating energy, but its increase makes the temperature of the air at the outlet of the TUR2 increase. The output cooling energy gradually decreases. When the X is greater than 0.4, the system has no cooling output. Considering the changes of the system's cooling output and output power comprehensively, the energy efficiency and the exergy efficiency of the CAES-GTCC increase after a period of decline. In the system design, the value of X can be taken considering the performance of the SC subsystem under off-design conditions. When the SC subsystem does not perform well under off-design conditions or when the demand for the output cooling energy is essential, it is recommended that X be set to 0.3. In other cases, it is recommended that X be set to a value greater than 0.5 to achieve better overall performance.

#### 4.3. Flow rate ratio of exhaust gas diverted from the heat source of CAES

The flow ratio of exhaust gas diverted from the heat source of CAES is defined as the ratio of the mass of exhaust gas entering the HX3 to the

total mass of exhaust gas used to heat the air in the CAES. It can be described as:  $Y = \frac{\dot{m}_{23}}{\dot{m}_{25}}$ . The effect of the flow rate ratio of exhaust gas diverted from the heat source of CAES on the system performance is indicated in Fig. 5. With the increase of the Y, the electrical efficiency of the CAES, the equivalent electric efficiency of the CAES-GTCC, the energy efficiency and the exergy efficiency of the CAES-GTCC increase after a period of decline. As the Y increases, the flow rate of the exhaust gas in HX3 increases; in contrast, the flow rate of the exhaust gas in HX4 decreases. When the Y increases, the output work of TUR1 decreases but the output work of TUR2 increases. The total output work of the CAES-GTCC decreases as the Y increases from 0.3 to 0.5 and increases as the Y increases from 0.5 to 0.7. The electrical efficiency of the CAES and the equivalent electric efficiency of the CAES-GTCC have the same trend as the total output work of the proposed system. As the Y increases, the temperature of the air at the outlet of the TUR2 increases. Specifically, the output cooling energy decreases when the Y increases from 0.3 to 0.55 and the system has no cooling output when the Y is greater than 0.55. Since the change of the Y does not affect the heating output, it is not difficult to find that the energy efficiency and the exergy efficiency of the CAES-GTCC both decrease at first and then increase after comprehensively considering the changes of the output power and cooling output of the coupled system. In the system design, the value of Y depends mainly on the demand for output cooling energy in the system. When the cooling energy is not required, it is recommended that Y be taken as 0.7 to output more power. When the cooling energy is needed, it is recommended that Y be taken as 0.3 to obtain more cooling energy while ensuring the comprehensive performance of the system.

#### 4.4. Efficiency of the air turbine

The effect of the efficiency of the air turbine on the system performance is revealed in Fig. 6. With the efficiency of the air turbine increases, the electrical efficiency of the CAES, the equivalent electric efficiency of the CAES-GTCC, the energy efficiency and the exergy efficiency of the CAES-GTCC increase. When the efficiency of the air turbine increases, the output work of TUR1 and TUR2 increases. Moreover, the total output work of the CAES-GTCC increases. Therefore, the electrical efficiency of the CAES and the equivalent electric efficiency of the CAES-GTCC increase, respectively. The heating output is not affected by changes of the efficiency of the air turbine. As the efficiency of the air turbine increases, the cooling output of the system increases due to the decrease of air temperature at the outlet of the TUR2. In addition, the system has no cooling output when the efficiency of the

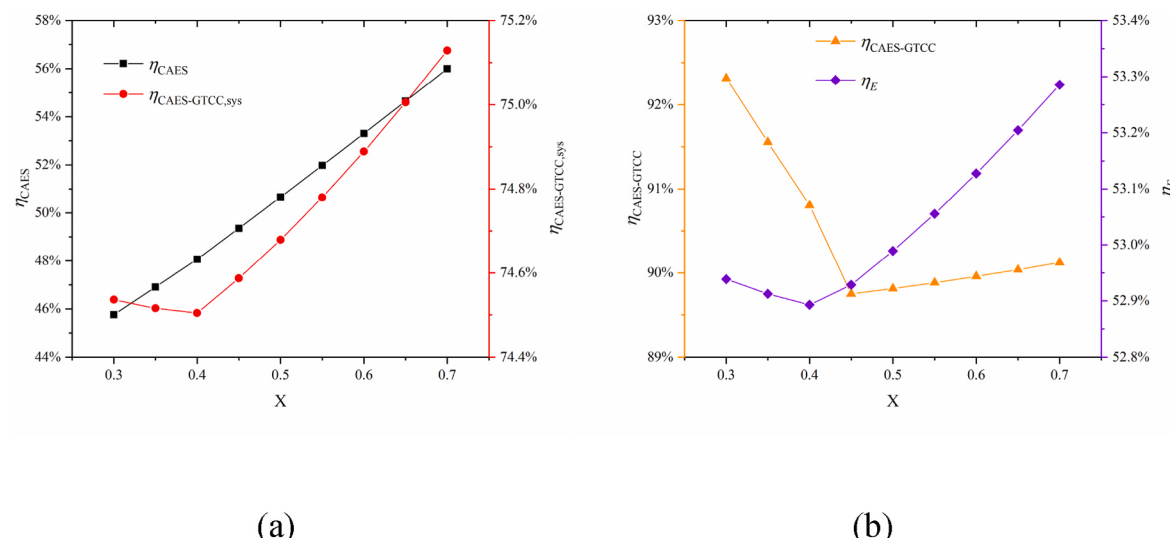


**Fig. 4.** Effect of the flow rate ratio of exhaust gas diverted from the HRSG on the system performance.

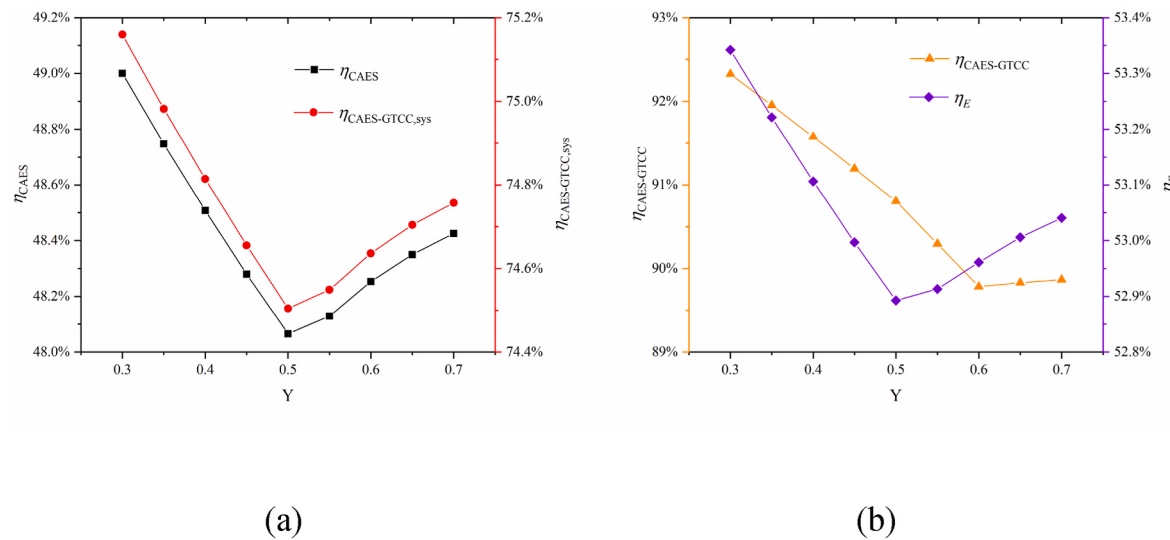


**Fig. 5.** Effect of the flow rate ratio of exhaust gas diverted from the heat source of CAES on the system performance.

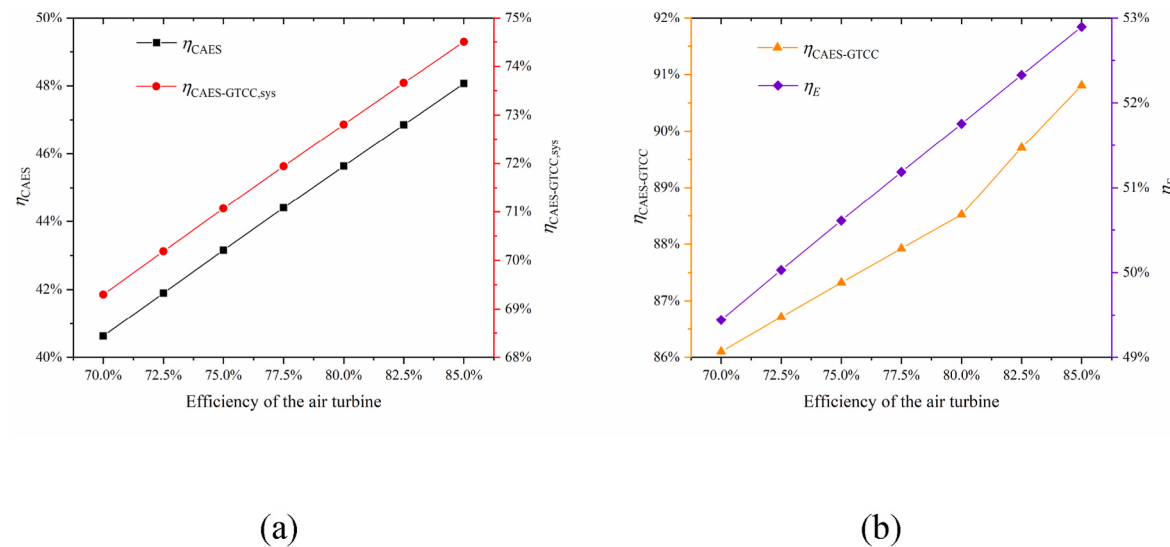


**Fig. 6.** Effect of the efficiency of the air turbine on the system performance.

air turbine is less than 82.5%. The changing trend of the whole useful energy output of the system (electricity, heating energy and cooling energy) is consistent with the changing trend of the total output work of the CAES-GTCC. Therefore, both the energy efficiency of the CAES-GTCC and the exergy efficiency of the CAES-GTCC increase with the increase of the efficiency of the air turbine. When selecting the equipment, the efficiency of the air turbine should be greater than 82.5% in order to ensure that the system has the ability to output cooling energy. Further, from a thermodynamic point of view, it is recommended that the efficiency of the air turbine be 85% so that the system can output more power and has the best thermodynamic performance.

#### 4.5. Outlet pressure of the cavern

The effect of the outlet pressure of the cavern on the system performance is shown in Fig. 7. As the outlet pressure of the cavern increases, the electrical efficiency of the CAES, the equivalent electric efficiency of the CAES-GTCC, the energy efficiency and the exergy efficiency of the CAES-GTCC increase. When the outlet pressure of the cavern increases, the output work of TUR1 and TUR2 increases due to

the increase of the pressure ratio of the TUR1 and TUR2. The total output work of the CAES-GTCC increases. The electrical efficiency of the CAES and the equivalent electric efficiency of the CAES-GTCC increase as the total output work of the CAES-GTCC increases. The heating output is not affected by changes of the outlet pressure of the cavern. As the pressure ratio of the TUR2 increases, the air temperature at the outlet of the TUR2 decreases, and the cooling output of the system increases. The total output energy, including output power, cooling out and heating output, increases. Therefore, the energy efficiency and the exergy efficiency of the CAES-GTCC increase.

#### 4.6. Inlet pressure of the cavern

The effect of the inlet pressure of the cavern on the system performance is given in Fig. 8. As the inlet pressure of the cavern increases, the electrical efficiency of the CAES, the equivalent electric efficiency of the CAES-GTCC and the exergy efficiency of the CAES-GTCC increase; in contrast, the energy efficiency of the CAES-GTCC decreases. With the increase of the inlet pressure of the cavern, the temperature of the air at the outlet of the COM1 and COM2 increases due to the increase of the

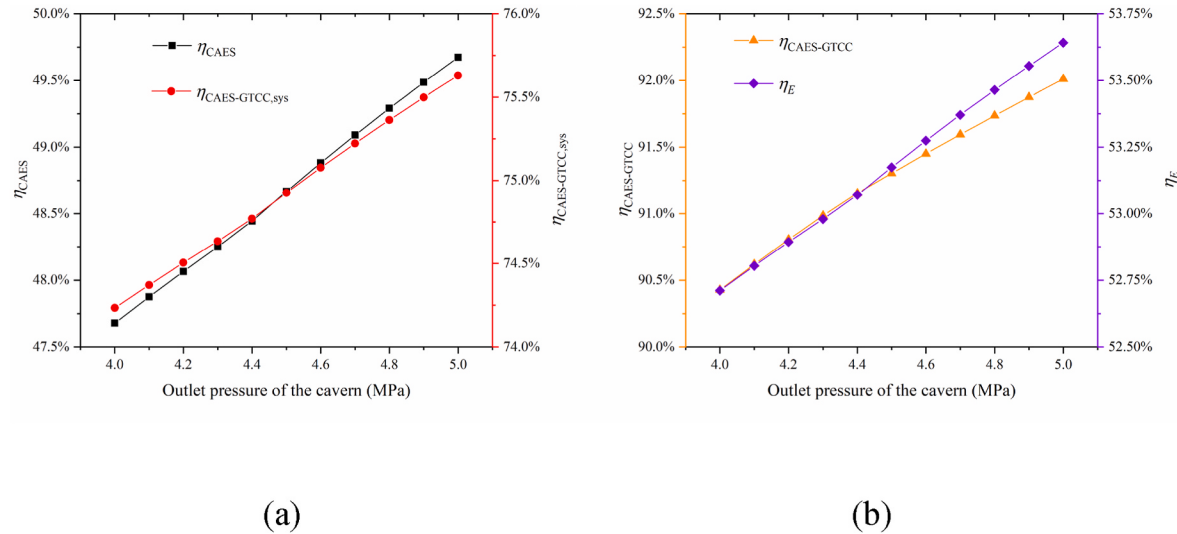


**Fig. 7.** Effect of the outlet pressure of the cavern on the system performance.

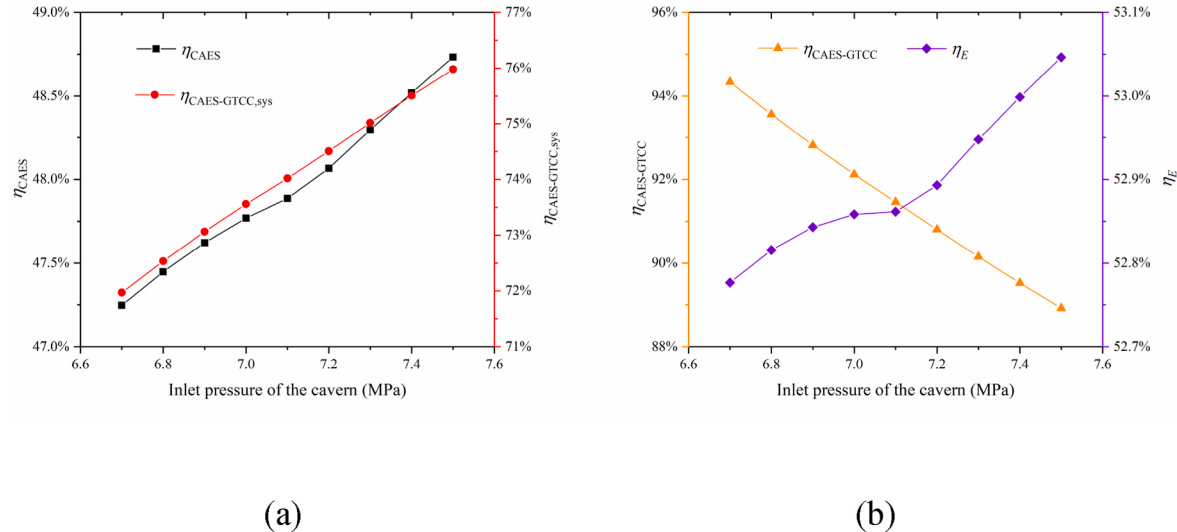


**Fig. 8.** Effect of the inlet pressure of the cavern on the system performance.

pressure ratio of COM1 and COM2. The flow rate of air in CR1 and CR2 decreases under the same heat exchange conditions. Therefore, the total input work of COM1 and COM2 decreases during charging. During discharging, the output work of TUR1, the output work of TUR2 and the total output work of the CAES-GTCC decrease due to the reduction of the quantity of the stored air. However, the change of the input work of COM1 and COM2 is greater than the change of the output work of TUR1 and TUR2. Therefore, the electrical efficiency of the CAES and the equivalent electric efficiency of the CAES-GTCC increase. When the flow rate of the exhaust gas in HX3 and HX4 remains constant, the temperature of the air at the outlet of the TUR2 increases, and the cooling output of the system decreases as the flow rate of the air decreases. The decrease of the flow rate of air in COM1 and COM2 causes a significant reduction of heating output when the inlet pressure of the cavern increases. The total output energy of cooling output, heating output and electricity of the coupled system is reduced, so the energy efficiency of the CAES-GTCC decreases. The decrease of heating output is the most significant, but the heating energy contains less exergy. The exergy efficiency of the CAES-GTCC increase, which is mainly affected by the change of output power.

#### 4.7. Reaction pressure of the cracking reaction

The effect of the reaction pressure of the cracking reaction on the system performance is illustrated in Fig. 9. The electrical efficiency of the CAES and the equivalent electric efficiency of the CAES-GTCC increase with the increase of the reaction pressure, but the energy efficiency and the exergy efficiency of the CAES-GTCC decrease. As the reaction pressure increases, the heat absorbed by methanol in the cracking reaction increases, and the flow rate of the air in COM1 and COM2 increases. When the flow rate of the CAES increases, the temperature of the air at the outlet of the TUR2 decreases and the cooling output of the CAES-GTCC increases. An increase of reaction pressure implies an increase of the pressure of the methanol at the outlet of the PUM1. The phase transition temperature of the methanol increases when the reaction pressure increases. The performance of methanol preheated by HRSG exhaust gas becomes worse. The proportion of compression heat used to preheat methanol increases. Accordingly, the heating output decreases. During charging, the pressure ratio of the COM3 decreases as the reaction pressure increases. The input work of COM3 decreases and the total input work of CAES decreases. As the pressure ratio of the COM3 decreases, the temperature of the cracked gas

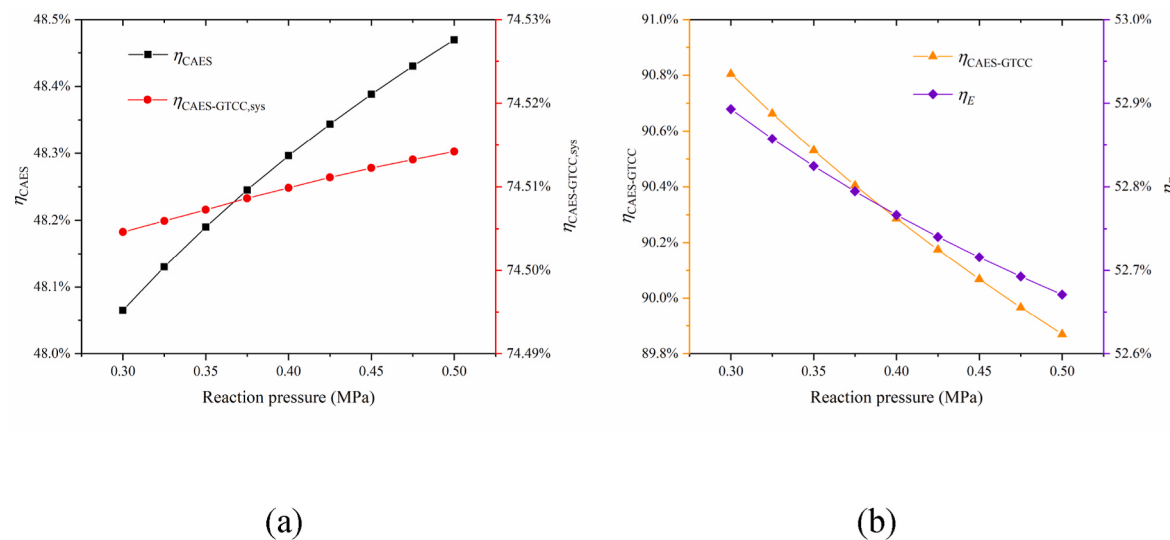


**Fig. 9.** Effect of the reaction pressure of the cracking reaction on the system performance.

entering the combustion chamber decreases. Further, the mass flow rate of the TUR3 decreases. As a result, the net output work of GTCC decreases. The output work of TUR1 and TUR2 decreases due to the decrease of the mass flow rate of the TUR3. The total output work of the CAES-GTCC decreases. However, the decrease of the total output work of the CAES-GTCC is less than the decrease of the total input work. The electrical efficiency of the CAES and the equivalent electric efficiency of the CAES-GTCC increase. Although there is a slight increase in cooling output, both the energy efficiency and exergy efficiency of the CAES-GTCC decrease in parallel.

#### 4.8. Efficiency of the air compressor in CAES

The effect of the efficiency of the air compressor in CAES on the system performance is shown in Fig. 10. With the efficiency of the air compressor in CAES increases, the electrical efficiency of the CAES and the equivalent electric efficiency of the CAES-GTCC decrease. In the meanwhile, the energy efficiency increases, and the exergy efficiency of the CAES-GTCC declines after a period of increase. As the efficiency of the air compressor in CAES increases, the temperature of the air at the outlet of the COM1 and COM2 decreases and the mass flow rate of the

CAES increases. The heating output increases when the input work of COM1 and COM2 increases. The temperature of the air at the inlet of the TUR1 and TUR2 decreases and the specific output work of the air turbine decreases considering that the mass flow rate of the air in HX3 and HX4 is increasing. Combining the factors of the increase of the mass flow rate of CAES and the decrease of the specific output work of air turbine, the output work of TUR1 and TUR2 increases. Therefore, the total output work of the CAES-GTCC increases. When the temperature of the air at the inlet of the TUR2 decreases, the temperature of the air at the outlet of the TUR2 decreases. When the efficiency of the air compressor in CAES is greater than 82.5%, the CAES-GTCC has cooling output. The increase of the total input work of CAES is greater than the increase of the total output work of the CAES-GTCC. Therefore, the electrical efficiency of the CAES and the equivalent electric efficiency of the CAES-GTCC decrease. The heating output of the CAES-GTCC increases substantially, so the energy efficiency of the CAES-GTCC increases. Considering that the total input work of CAES is increasing and the total output work of the CAES-GTCC and heating output are increasing obviously, the exergy efficiency of CAES-GTCC shows a trend of increasing first and then decreasing. When selecting equipment, the efficiency of the air compressor in CAES is recommended to be 85% to

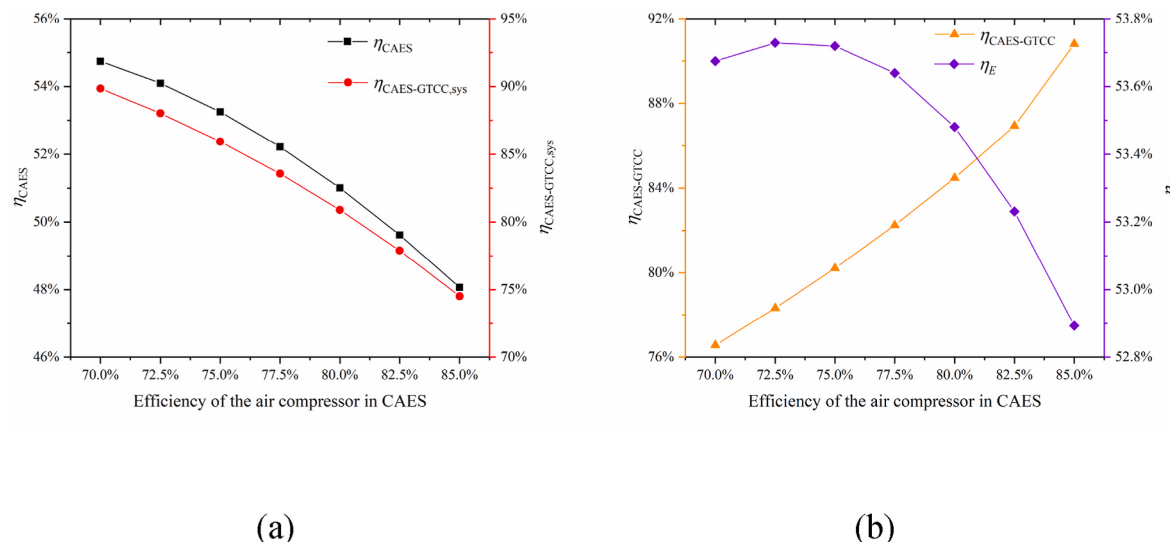


**Fig. 10.** Effect of the efficiency of the air compressor in CAES on the system performance.

ensure that the system has sufficient capacity to output cooling energy. When there is no demand for cooling energy, the efficiency of the air compressor in CAES is recommended to be around 72.5% to make the coupled system have a satisfactory exergy efficiency.

#### 4.9. Pressure ratio of the gas cycle

The effect of the pressure ratio of the GC on the system performance is revealed in Fig. 11. As the pressure ratio of the GC increases, the equivalent electric efficiency of the CAES-GTCC, the energy efficiency of the CAES-GTCC and the exergy efficiency of the CAES-GTCC increase. At the same time, the electrical efficiency of the CAES decreases when the pressure ratio of the GC increases from 10 to around 14. While the pressure ratio of the GC increases from 14 to 15, the electrical efficiency of the CAES increases slowly. With the pressure ratio of the GC increases, the total net output work of the GTCC and the total output work of the CAES-GTCC increase. The temperature of the air at the outlet of the TUR2 decreases and the cooling output of the CAES-GTCC increases when the pressure ratio of the GC increases. The total input work of CAES increases due to the increase of the pressure ratio of the COM3. The mass flow rate of the exhaust gas in HRSG increases and the temperature of the exhaust gas at the outlet of the HRSG increases. The heat of the exhaust gas absorbed by methanol during preheating increases and the proportion of compression heat used to preheat methanol decreases. Therefore, the heating output of the CAES-GTCC increases. Several performance criteria of the proposed system show a complex variation considering the changes of the output power, heating output and cooling output of the CAES-GTCC comprehensively.

#### 4.10. Discussion

It is obvious that the heating output of the CAES-GTCC is much more than the cooling output. It should be emphasized that the ratio of heating output and cooling output of the CAES-GTCC can be adjusted by using the compression heat of the air in HX1 or HX2 to drive the ejector refrigeration cycle. To simplify the calculation and analysis, a single-pressure GTCC without reheat is selected in this paper. With a more advanced GTCC (e.g., double-pressure GTCC with reheat), the proposed system will be expected to obtain better comprehensive performance. In this system, the application of the thermal energy storage system in CAES is avoided by combining the cracking reaction of methanol to absorb the compression heat. However, the compression heat cannot be fully reused in the cracking reaction of methanol. A part of the

compression heat is exported through heating energy. This reveals that the generation of compression heat can be avoided in the case of utilizing isothermal compression techniques. By combining I-CAES with GTCC, system performance will be further improved. In particular, the flexibility of the electricity, heating energy and cooling energy of the coupled system will be effectively improved.

According to the principle of this system, the system can be miniaturized combined with the specific application scenarios. For the scale of the system in this paper, we mainly consider building the system near an industrial park with methanol production conditions, such as Yulin City, Shaanxi Province, China. Such considerations not only facilitate methanol delivery but also provide energy storage and power support for nearby industrial parks through this system.

#### 5. Conclusions

In this paper, a system coupled with CAES and GTCC is proposed, which has a large-scale peak shaving capability. The compression heat is absorbed by the cracking reaction of the methanol in this system avoiding the application of thermal energy storage devices in the CAES system. During discharging, part of the gas diverted from the GTCC heats the air that is about to enter the air turbine in CAES. Moreover, the CAES-GTCC system can realize the energy cascade utilization by outputting various forms of energy including cooling energy, heating energy and electricity.

The detailed thermodynamic models of each component have been built. Based on the first law of thermodynamics and the second law of thermodynamics, thermodynamic analysis and sensitivity analysis of the proposed system have been carried out. Based on the single-pressure GTCC without reheat, the electrical efficiency of the CAES, the equivalent electric efficiency of the CAES-GTCC and the energy efficiency of the CAES-GTCC could reach 48.07%, 74.51% and 90.81%, respectively. In the perspective of the second law of thermodynamics, the exergy efficiency of the CAES-GTCC is expected to reach about 52.89%. It is worth noting that the total output power of CAES-GTCC during discharging accounted for 157.09% of the total output power during the general period. Moreover, the system has no cooling output when the efficiency of the air compressor in CAES or the efficiency of the air turbine is not satisfactory. When the performance of the SC is worse under off-design conditions, the flow rate ratio of exhaust gas diverted from the HRSG, X, is recommended to choose 0.3.

Sensitivity analysis is of great significance for researchers to deeply understand the system. The results in this paper contribute to the

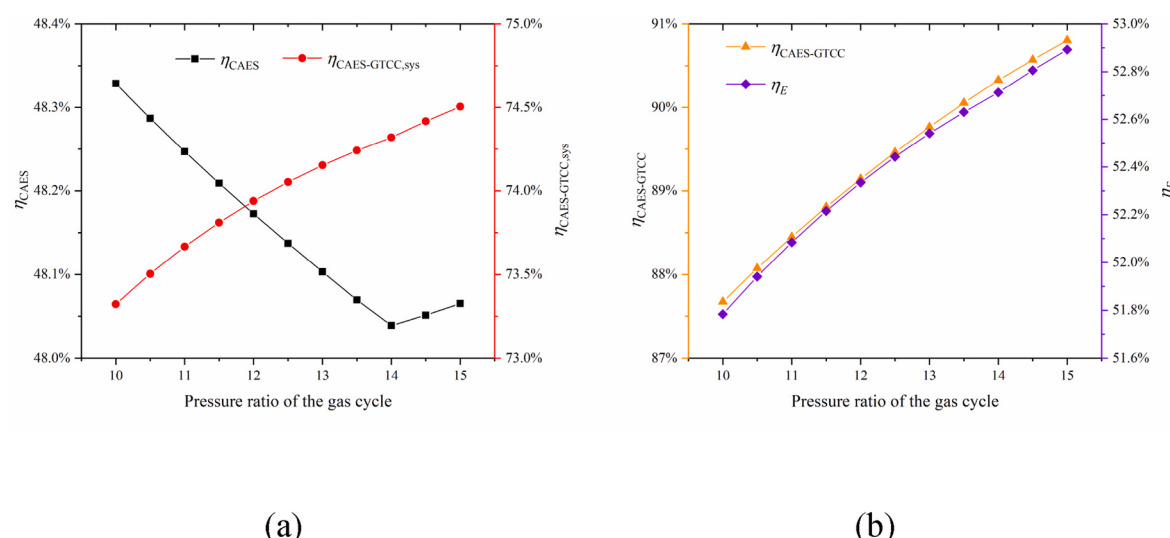


Fig. 11. Effect of the pressure ratio of the gas cycle on the system performance.

development of EES, especially CAES. Furthermore, a concept of the system combining I-CAES with GTCC is inspired based on the research in this paper.

## Credit author statement

He, Xin He: Investigation, Formal analysis, Methodology, Software, Writing, Chengchen Li: Methodology, Formal analysis, Huanran Wang: Supervision, Resources, Funding acquisition.

## Declaration of competing interest

The authors declare that they have no known competing financial interests or personal relationships that could have appeared to influence the work reported in this paper.

## Data availability

Data will be made available on request.

## Acknowledgments

The authors are grateful to the support provided by the National Natural Science Foundation of China (No. 51676151).

## References

- [1] Li Ruixiong, Zhang Haoran, Chen Hao, Zhang Yan, Li Zhibo, Zhao Jing, Wang Xuejun, Wang, Huanran. Hybrid techno-economic and environmental assessment of adiabatic compressed air energy storage system in China-Situation. *Appl Therm Eng* 2021;186.
- [2] Li Peng, Hu Qingya, Han Zhonghe, Wang Changxin, Wang Runxia, Han Xu, Wang Yongzhen. Thermodynamic analysis and multi-objective optimization of a trigenerative system based on compressed air energy storage under different working media and heating storage media. *Energy* 2022;239.
- [3] Zhang Xuelin, Zhang Tong, Ma Linrui, Wen Jun, Wang Guohua, Wang Bin, Mei Shengwei, Gong Linghui, Xue Xiaodai. Cogeneration compressed air energy storage system for industrial steam supply. *Energy Convers Manag* 2021;235.
- [4] Olabi AG, Onumaegbu C, Wilberforce Tabbi, Ramadan Mohamad, Abdelkareem Mohammad Ali, Alami Al -, Abdul Hai. Critical review of energy storage systems. *Energy* 2021;214.
- [5] Zheng Yingying, Sahraei-Ardakani, Mostafa. Leveraging existing water and wastewater infrastructure to develop distributed pumped storage hydropower in California. *J Energy Storage* 2021;34.
- [6] Emmanouil Stergios, Nikolopoulos Eftymios I, François Baptiste, Brown Casey, Anagnostou Emmanouil N. Evaluating existing water supply reservoirs as small-scale pumped hydroelectric storage options – a case study in Connecticut. *Energy* 2021;226.
- [7] Pérez-Díaz, Juan I, Chazarra M, García-González J, Cavazzini G, Stoppato A. Trends and challenges in the operation of pumped-storage hydropower plants. *Renew Sustain Energy Rev* 2015;44:767–84.
- [8] Chen Haisheng, Cong Thang Ngoc, Yang Wei, Tan Chunqing, Li Yongliang, Ding, Yulong. Progress in electrical energy storage system: a critical review. *Prog Nat Sci* 2009;19(3):291–312.
- [9] Zhang Shuyu, Wang Huanran, Li Ruixiong, Li Chengchen, Hou Fubin, Ben Yue. Thermodynamic analysis of cavern and throttle valve in large-scale compressed air energy storage system. *Energy Convers Manag* 2019;183:721–31.
- [10] Tong Zheming, Cheng Zhenwu, Tong Shuiwang. A review on the development of compressed air energy storage in China: technical and economic challenges to commercialization. *Renew Sustain Energy Rev* 2021;135.
- [11] Rahmanifard Hamid, Plaksina Tatyana. Hybrid compressed air energy storage, wind and geothermal energy systems in Alberta: feasibility simulation and economic assessment. *Renew Energy* 2019;143:453–70.
- [12] Ni C, Xue X, Mei S, Zhang XP, Chen X. Technological research of a clean energy router based on advanced adiabatic compressed air energy storage system. *Entropy* 2020;22(12).
- [13] Borri Emiliiano, Tafone Alessio, Romagnoli Alessandro, Comodi Gabriele. A review on liquid air energy storage: history, state of the art and recent developments. *Renew Sustain Energy Rev* 2021;137.
- [14] Zhou Shenghui, He Yang, Chen Haisheng, Xu Yujie, Deng Jianqiang. Performance analysis of a novel adiabatic compressed air energy system with ejectors enhanced charging process. *Energy* 2020;205.
- [15] Liu Mingming, Wang Huanran, Li Ruixiong, Du Chaoyun, Li Chengchen, Yan Kai. Thermodynamic analysis of an isobaric compressed air energy storage (I-CAES) combined with low grade waste heat. *IOP Conf Ser Earth Environ Sci* 2019;227.
- [16] Luo Xing, Wang Jihong, Krupke Christopher, Wang Yue, Sheng Yong, Li Jian, Xu Yujie, Wang Dan, Miao Shihong, Chen Haisheng. Modelling study, efficiency analysis and optimisation of large-scale Adiabatic Compressed Air Energy Storage systems with low-temperature thermal storage. *Appl Energy* 2016;162:589–600.
- [17] Koohi-Fayegh S, Rosen MA. A review of energy storage types, applications and recent developments. *J Energy Storage* 2020;27.
- [18] Zhou Qian, Du Dongmei, Lu Chang, He Qing, Liu Wenyi. A review of thermal energy storage in compressed air energy storage system. *Energy* 2019;188.
- [19] Wu Danman, Bai Jiayu, Wei Wei, Chen Laijun, Mei Shengwei. Optimal bidding and scheduling of AA-CAES based energy hub considering cascaded consumption of heat. *Energy* 2021;233.
- [20] Courtois Nicolas, Najafiyazdi Mostafa, Lotfalian Reza, Boudreault Richard, Picard Mathieu. Analytical expression for the evaluation of multi-stage adiabatic-compressed air energy storage (A-CAES) systems cycle efficiency. *Appl Energy* 2021;288.
- [21] Jubeh Naser M, Najjar Yousef SH. Green solution for power generation by adoption of adiabatic CAES system. *Appl Therm Eng* 2012;44:85–9.
- [22] Wang Sixian, Zhang Xuelin, Yang Luwei, Zhou Yuan, Wang Junjie. Experimental study of compressed air energy storage system with thermal energy storage. *Energy* 2016;103:182–91.
- [23] Yao Erren, Wang Huanran, Wang Ligang, Xi Guang, Maréchal François. Thermo-economic optimization of a combined cooling, heating and power system based on small-scale compressed air energy storage. *Energy Convers Manag* 2016;118: 377–86.
- [24] Chen Hao, Wang Huanran, Li Ruixiong, Sun Hao, Ge Gangqiang, Ling Lanning. Experimental and analytical investigation of near-isothermal pumped hydro-compressed air energy storage system. *Energy* 2022;249.
- [25] Li Ruixiong, Wang Huanran, Tu Qingshi. Thermo-economic analysis and optimization of adiabatic compressed air energy storage (A-CAES) system coupled with a Kalina cycle. *Energy Technol* 2018;6(6):1011–25.
- [26] Zhong Like, Yao Erren, Hu Yang, Zhao Chenxi, Zou Hansen, Xi Guang. Thermo-economic analysis of a novel system integrating compressed air and thermochemical energy storage with solid oxide fuel cell-gas turbine. *Energy Convers Manag* 2022;252.
- [27] DinAli Magd N, Dincer Ibrahim. Development and analysis of an integrated gas turbine system with compressed air energy storage for load leveling and energy management. *Energy* 2018;163:604–17.
- [28] Jannelli E, Minutillo M, Lubrano Lavadera A, Falucci G. A small-scale CAES (compressed air energy storage) system for stand-alone renewable energy power plant for a radio base station: a sizing-design methodology. *Energy* 2014;78: 313–22.
- [29] Mohammadi Amin, Mehrpooya Mehdi. Exergy analysis and optimization of an integrated micro gas turbine, compressed air energy storage and solar dish collector process. *J Clean Prod* 2016;139:372–83.
- [30] Wang Xusheng, Yang Cheng, Huang Manman, Ma Xiaoqian. Off-design performances of gas turbine-based CCHP combined with solar and compressed air energy storage with organic Rankine cycle. *Energy Convers Manag* 2018;156: 626–38.
- [31] Yang Cheng, Huang Zhifeng, Ma Xiaoqian. Comparative study on off-design characteristics of CHP based on GTCC under alternative operating strategy for gas turbine. *Energy* 2018;145:823–38.
- [32] Choi Ju Hwan, Ahn Ji Ho, Kim Tong Seop. Performance of a triple power generation cycle combining gas/steam turbine combined cycle and solid oxide fuel cell and the influence of carbon capture. *Appl Therm Eng* 2014;71(1):301–9.
- [33] He Xin, Wang Huanran, Li Ruixiong, Sun Hao, Chen Hao, Li ChengChen, Ge Gangqiang, Tao, Feiyue. Thermo-conversion of a physical energy storage system with high-energy density: combination of thermal energy storage and gas-steam combined cycle. *Energy* 2022;239.
- [34] Salvini Coriolano. CAES systems integrated into a gas-steam combined plant: design point performance assessment. *Energies* 2018;11(2).
- [35] Kim Min Jae, Kim Tong Seop. Integration of compressed air energy storage and gas turbine to improve the ramp rate. *Appl Energy* 2019;247:363–73.
- [36] Wojcik Jacek D, Wang Jihong. Feasibility study of combined cycle gas turbine (CCGT) power plant integration with adiabatic compressed air energy storage (ACAES). *Appl Energy* 2018;221:477–89.
- [37] Jeong Ji Hun, Yi Ji Hye, Kim Tong Seop. Analysis of options in combining compressed air energy storage with a natural gas combined cycle. *J Mech Sci Technol* 2018;32(7):3453–64.
- [38] Yang Cheng, Wang Xusheng, Huang Manman, Ding Su, Ma Xiaoqian. Design and simulation of gas turbine-based CCHP combined with solar and compressed air energy storage in a hotel building. *Energy Build* 2017;153:412–20.
- [39] Liu Taixiu, Liu Qibin, Lei Jing, Sui Jun, Jin Hongguang. Solar-clean fuel distributed energy system with solar thermochemistry and chemical recuperation. *Appl Energy* 2018;225:380–91.
- [40] Liu Xiangyu, Hong Hui, Zhang Hao, Cao Yali, Qu Wanjun, Jin Hongguang. Solar methanol by hybridizing natural gas chemical looping reforming with solar heat. *Appl Energy* 2020;277.
- [41] Wang Jiangjiang, Han Zepeng, Guan Zhimin. Hybrid solar-assisted combined cooling, heating, and power systems: a review. *Renew Sustain Energy Rev* 2020; 133.
- [42] Zheng Zhimei, Liu Taixiu, Liu Qibin, Lei Jing, Fang Juan. A distributed energy system integrating SOFC-MGT with mid-and-low temperature solar thermochemical hydrogen fuel production. *Int J Hydrogen Energy* 2021;46(38): 19846–60.
- [43] Razmi Amir Reza, Janbaz Majid. Exergoeconomic assessment with reliability consideration of a green cogeneration system based on compressed air energy storage (CAES). *Energy Conversion and Management*; 2020. p. 204.

- [44] Li Ruixiong, Wang Huanran, Zhang Haoran. Dynamic simulation of a cooling, heating and power system based on adiabatic compressed air energy storage. *Renew Energy* 2019;138:326–39.
- [45] Zare V, Moalemin A. Parabolic trough solar collectors integrated with a Kalina cycle for high temperature applications: energy, exergy and economic analyses. *Energy Convers Manag* 2017;151:681–92.
- [46] Wang Hongsheng, Liu Mingkai, Kong Hui, Hao Yong. Thermodynamic analysis on mid/low temperature solar methane steam reforming with hydrogen permeation membrane reactors. *Appl Therm Eng* 2019;152:925–36.
- [47] Xu Da, Liu Qibin, Lei Jing, Jin Hongguang. Performance of a combined cooling heating and power system with mid-and-low temperature solar thermal energy and methanol decomposition integration. *Energy Convers Manag* 2015;102:17–25.
- [48] Cheayb Mohamad, Gallego Marin, Mylène, Tazerout Mohand, Poncet Sébastien. Modelling and experimental validation of a small-scale trigenerative compressed air energy storage system. *Appl Energy* 2019;239:1371–84.
- [49] Liu Wenyi, Li Qing, Liang Feifei, Liu Linzhi, Xu Gang, Yang Yongping. Performance analysis of a coal-fired external combustion compressed air energy storage system. *Entropy* 2014;16(11):5935–53.
- [50] Odibi Chukwuka, Babaie Meisam, Zare Ali, Nabi Md Nurun, Bodisco Timothy A, Brown Richard J. Exergy analysis of a diesel engine with waste cooking biodiesel and triacetin. *Energy Conversion and Management*; 2019. p. 198.
- [51] Fateh Sana. Bi-directional Solid Oxide Cells used as SOFC for Aircraft APU system and as SOEC to produce fuel at the airport. 2016.

## Glossary

*E*: Exergy, J  
*h*: Specific enthalpy, J/kg  
*LHV*: Low heating value, J/kg  
 $\dot{m}$ : Mass flow rate, kg/s  
*M*: Mass, kg  
*P*: Pressure, MPa  
 $q$ : Heat per unit mass, J/kg  
*Q*: Heat, J  
*t*: Time, s  
*W*: Power, W  
*W*: Work, J  
*X, Y*: Flow rate ratio

## Greek symbols

$\varepsilon$ : Pressure ratio  
 $\eta$ : Efficiency  
 $\varphi$ : Exergy factor of fuel  
 $\omega$ : Mass fraction

## Acronyms

A: CAES Adiabatic compressed air energy storage  
 CAES: Compressed air energy storage  
 CAES-GTCC: Compressed air energy storage integrated with gas-steam combined cycle  
 CC: Combustion chamber  
 CCHP: Combined cooling, heating and power  
 COM: Compressor  
 CON: Condenser  
 CR: Cracking reactor  
 DCAES: Diabatic compressed air energy storage  
 EES: Electrical energy storage  
 GC: Gas cycle  
 GTCC: Gas-steam combined cycle  
 HRSG: Heat recovery steam generator  
 HX: Heat exchanger  
 I-CAES: Isothermal compressed air energy storage  
 LAES: Liquid air energy storage  
 PHES: Pumped hydro energy storage  
 PUM: Pump  
 SC: Steam cycle  
 THV: Throttle valve  
 TUR: Turbine

## Subscripts and superscripts

*a*: Air that did not participate in the combustion reaction  
*c*: Substances involved in combustion reactions  
 CAES: Compressed air energy storage  
 CAES-GTCC: Compressed air energy storage integrated with gas-steam combined cycle  
*CH*: Methanol  
 COM: Compressor  
 CON: Condenser  
*cooling*: Cooling energy  
*E*: Exergy  
 GC: Gas cycle  
 GTCC: Gas-steam combined cycle  
*heating*: Heating energy  
*input*: Input  
*output*: Output  
*P*: Product  
*power*: Electricity  
 PUM: Pump  
*R*: Reactant  
*s*: Isentropic process  
 SC: Steam cycle  
*sys*: The conversion of heat to electricity in a system  
*T*: Temperature  
 TUR: Turbine  
*0*: Reference state of thermochemical standard